ACCELERATED THREE DIMENSIONAL RAY TRACING TECHNIQUES USING RAY FRUSTUMS FOR WIRELESS PROPAGATION MODELS

H. Kim and H. Lee

Department of Electronic Engineering
Sogang University
Seoul, Korea

Abstract—In this paper, accelerated techniques for three dimensional ray tracing using the concept of ray frustums are presented for the fast characterization of wireless communications, where various radio propagation paths such as wall-transmitted wave and scattered wave from buildings and ground are generated. To accommodate such scatterers, objects are modeled by triangulated meshes, and potential ray paths are searched and stored in the form of ray frustums. The presented acceleration techniques using the frustums include sorting of triangulated surfaces, hashing functions and space partitioning. The validity of the method is verified by comparison with measurement data.

1. INTRODUCTION

As various wireless communication services are available for indoor and outdoor services, the demand for an accurate propagation model for radio waves increases. The traditional radio propagation models include a simple free space model, a ground reflection model, and statistical models such as Hata's or Okumura's. Those models are simple to use but do not give site-specific prediction, requiring supplementary on-site measurement data. To overcome those problems, more quantitative models that consider environment information about buildings, walls, windows and furniture are developed and widely adopted. Examples of the models are based on geometrical optics [1–5], uniform theory of diffraction (UTD) [6, 7], hybrid moment method [8], and FDTD [9]. Of those, ray tracing techniques combined with UTD are most frequently used. In

---

Corresponding author: H. Lee (leehs95@sogang.ac.kr).

those techniques, ray paths are searched first and utilized to obtain propagation loss, delay spread, and other parameters at numerous receiving positions. In most cases, indoor or outdoor environments are divided into mesh surfaces [10], and potential ray paths are searched by a number of ray-surface intersection tests using shooting and bouncing ray (SBR) method [3, 4] or those of ray tubes [7]. The ray-surface intersection tests are the most time consuming routine of ray tracing based propagation models. To accelerate the process, various space partitioning methods such as angular sectoring [6], kD-tree, octree, quad tree [11–13] and a preprocessing method are proposed [14]. In computer graphics field also, acceleration techniques for the visibility test have been studied, in which the concept of ray frustums [15] was introduced to accelerate the visibility tests in generating graphic images, and the concept is applied to radio [16] and sound wave [17] propagations.

In this paper, acceleration techniques adopting ray frustums combined with triangular meshes are proposed for fast three dimensional wave propagation modeling. The frustum represents a region that contains every possible ray path after scattering from an object and enables to find a ray path from a source to a receiver, reducing unnecessary ray launching or ray-surface intersection tests. In the following sections, ray frustums for line of sight ray paths, reflected, transmitted, and diffracted waves are described in detail, and acceleration techniques using them are explained. A comparison with measured data and computational efficiency are also presented.

2. RAY TRACING USING RAY FRUSTUMS

The generation of ray frustums is closely related to environment modeling data. In Fig. 1, a wireless communication environment is tessellated into triangular surfaces [10] to facilitate ray-object intersection tests and ray frustum generation. With the triangulated surfaces, ray-object intersection tests can be performed by a simple ray-triangle intersection test algorithm. For efficient calculations, the triangulation should be done such that only two triangles meet on an edge. This is because ray frustums generated from scattering triangular meshes divide free space into a set of discrete regions without overlapping.

After the environment data are loaded, the ray tracing process begins. For modeling a scattered wave from an obstacle, a ray frustum is formed with the visible triangular surface as a base. The apex of the frustum is set by the source position. The ray frustum represents a region that contains all the candidate ray paths scattered from the
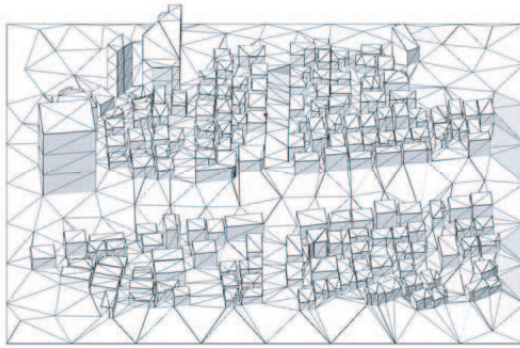
Figure 1. Triangulated surfaces of an outdoor environment. Buildings and grounds are tessellated.

triangular surface. Fig. 2 shows a ray frustum that contains all the reflected ray paths from the triangle of the obstacle. The region is defined by planes that are constructed from edges of the triangle and an image source. If an observation point is included in the frustum, a ray path is easily determined. The hit point on the triangle is the intersection point of a line that connects the real or virtual source and the observation point. If the ray is not obstructed by other triangles, reflected waves through the path arrive at the observation point. Since ray frustums are formed on visible triangles only, unnecessary ray launching is minimized. Subsequent ray frustums may be generated by the obstacles that intercept the ray frustum. The frustums are stored in a computer memory and utilized to determine the whole ray paths from the transmitter to a receiver. Although a large computer memory seems to be required for complex environments, dynamic allocation of memory usage allows us to perform simulations on a personal computer with moderate memory size.

Ray frustums are classified by the scattering mechanisms. As mentioned previously, four kinds of frustums are generated according to the origin of the scattered waves.

The first generated ray frustums are for the line of sight ray paths. To accommodate every possible ray path from a transmitter, the line of sight frustums should cover a whole free space with the source at the location of the transmitter. For computational efficiency, the free space is divided into a number of wedge shaped regions that extend vertically and radially to infinity (Fig. 3). The regions are defined as line of sight ray frustums. The shape is chosen for partitioning obstacles; most of which are spread horizontally. This partitioning allows us to reduce the number of calculation needed for the ray-triangle intersection test.
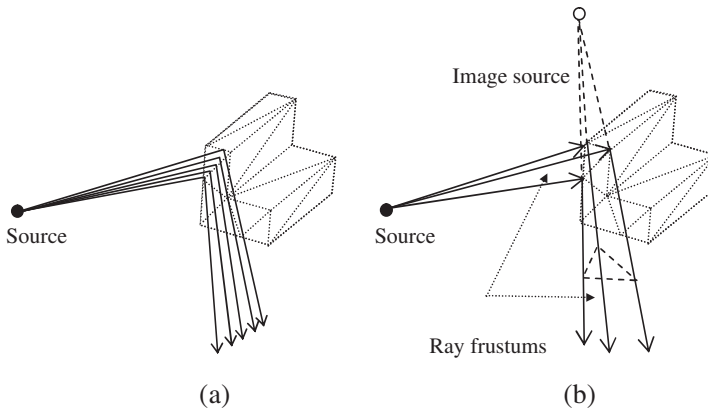
Figure 2. A ray frustum represents collectively all ray paths possible scattered from a triangle. (a) Actual ray paths reflected from a triangle surface, (b) a ray frustum enclosed by planes defined by the image source and edges of the visible triangle.
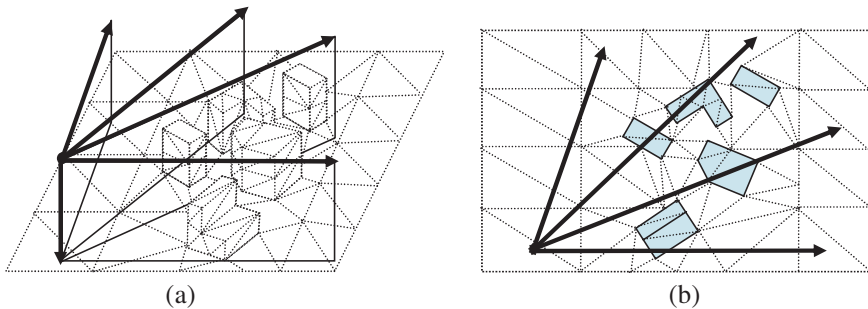

Figure 3. Space divisions for line of sight ray frustums. (a) Ray frustums for line of sight ray paths, (b) top view.

Suppose that the number of wedge shaped regions is N. The rays emitted from the source are scattered by the triangulated surfaces. It is assumed that the surfaces are composed of n triangles. A visibility test should be performed to determine whether a triangular surface receives a line of sight ray from the source. In each test, it is determined whether a line segment connecting the source, and the center point of a triangle intersects other triangles. If the space is not divided into N regions, the number of calculation needed is $n(n-1)$ for exhaustive search of the visible triangles. With N divisions, the average number of triangles in each division is n/N. Then the number of calculation

is reduced to $(n/N)(n/N-1)N \approx n^2/N$. Due to the space division, a reduction by a factor of N is achieved. This reduction is effective unless the number N is too large. If the number exceeds a certain limit, the wedge shaped regions become so narrow, and triangles of the obstacles tend to belong to several adjacent regions, thus increasing computation time.

The region of a ray frustum is specified by a number of planes. For each plane, the normal vector $\hat{\mathbf{n}}$ and a position vector should be specified and stored in memory. The normal vector is directed to the outside of the ray frustum. To determine whether the i-th triangle is included in a ray frustum, distances from the center of mass point $\mathbf{r}_{c,i}$ of the triangle to the planes are calculated by simple dot products, as shown in Fig. 4. If the distance is larger than the radius r_i of the bounding sphere [14], it can be safely assumed that the triangle is outside the frustum. The condition is satisfied by Eq. (1).

$$(\mathbf{r}_{c,i} - \mathbf{s}) \bullet \hat{\mathbf{n}}_{1,2} - r_i > 0 \tag{1}$$

Among the included triangles, triangles visible from the source are used to generate ray frustums that contain scattered waves. For reflected wave, the frustum region has boundaries defined by a visible triangle and planes made from the vertices of edges and the image source point. The frustum region extends away from the triangle. Fig. 5 shows ray frustums generated from triangular surfaces visible from the source.

Diffracted waves can also be modeled by frustums. The edges of the visible triangles generate diffracted waves. This fact can be utilized to form frustum regions that diffracted waves can reach. Fig. 6 shows frustum regions bounded by diffraction cones and planes that divide the region into sectors. The division is aimed to reduce the computation time for visibility tests. For a receiving point included
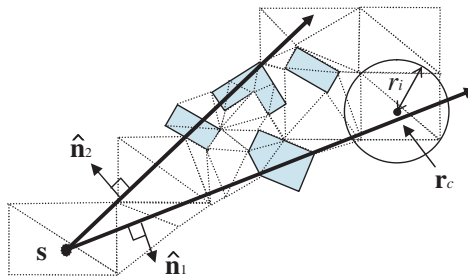

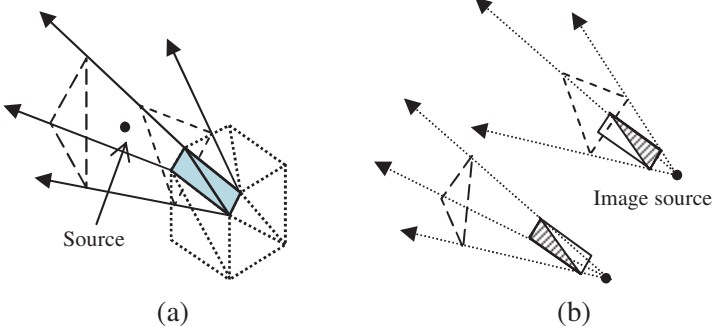**Figure 4.** Triangles which intersect a ray frustum can be chosen by a simple test.

Figure 5. Generation of ray frustums for reflected waves. (a) Ray frustums for reflected waves, (b) each frustum is generated by vertices of the illuminated triangle and its image source point.
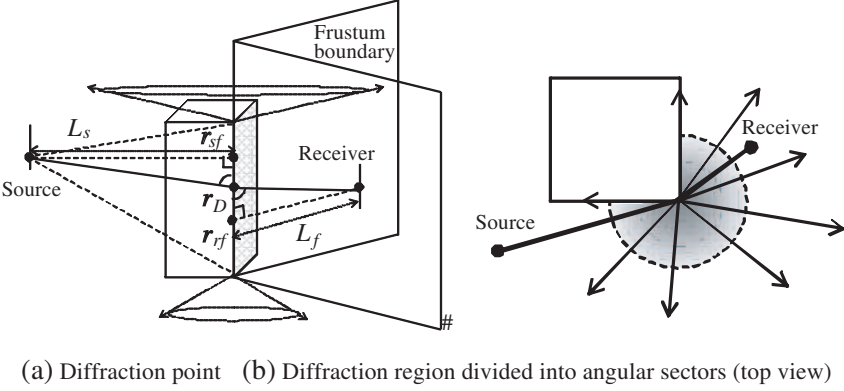

(a) Diffraction point   (b) Diffraction region divided into angular sectors (top view)

Figure 6. A ray frustum for diffracted waves. (a) Diffraction occurs due to edges of triangles which are illuminated by real or virtual sources, (b) ray frustums for the diffracting edge are generated by sectoring the region bounded by diffraction cones.

in a diffraction frustum, the diffraction point $\mathbf{r}_D$ satisfying the law of diffraction can be obtained by Eq. (2), where $\mathbf{r}_{sf}$ and $\mathbf{r}_{rf}$ are the feet of the source and the receiver position perpendicular to the edge. The distance L_s is the distance from the source to $\mathbf{r}_{sf}$. Likewise, L_f is the distance from the receiver position to the foot $\mathbf{r}_{rf}$.

$$\mathbf{r}_D = \frac{L_s \mathbf{r}_{rf} + L_f \mathbf{r}_{sf}}{L_s + L_f} \tag{2}$$

With the ray path set, scattered field vectors can be calculated using the formulas in [3, 18].
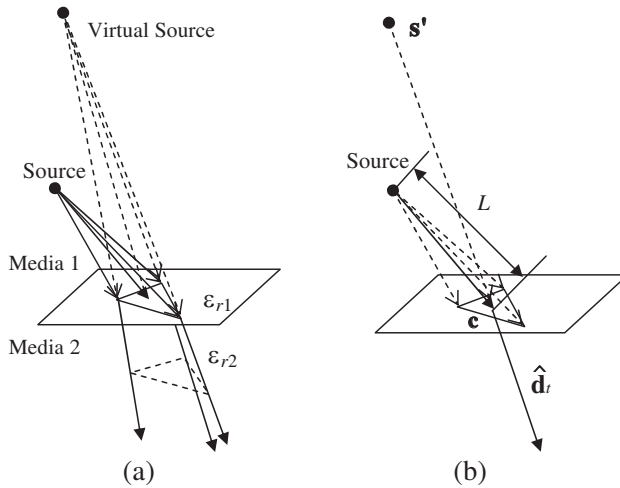
Figure 7. Generation of ray frustums for transmit waves. Refracting effect can be modeled approximated by a virtual source position. (a) Transmit ray frustum, (b) virtual source point of the frustum.

Transmitted rays can also be modeled by frustums, as shown in Fig. 7. A transmission ray frustum can be generated with a visible triangle, if the triangular surface is of transmissive medium. On entering a different medium, the incident wave refracts according to Snell's law. A virtual source position for transmitted wave is introduced to determine ray paths approximately. The transmitted wave propagates as if it originated from the virtual source position. The position can be obtained by the following Eq. (3).

$$\mathbf{s}' = \mathbf{c} - L\sqrt{\frac{\varepsilon_{r2}}{\varepsilon_{r1}}} \cdot \hat{\mathbf{d}}_t \qquad (3)$$

where $\mathbf{c}$ is the center of mass point of the visible triangle, and L is the distance from the real source to the center of mass point. The relative permittivity of the medium containing the source is ε_{r1}. That of the transmissive medium is ε_{r2}. The direction vector of the transmitted wave that propagates through the center of mass point is $\hat{\mathbf{d}}_t$. The ray frustum for the transmitted wave has boundaries defined by four planes including the visible triangle, planes determined by the virtual source point and each edge of the triangle.

With the ray frustums generated and stored in the computer memory, received electric fields at various observation points can be obtained. First, it should be examined whether an observation point is included in a ray frustum. Then, we should trace back to the source

point from the observation point to see if the ray path is not intercepted by obstacles. If the ray path is not obstructed, the received field contribution is computed and added. The process should be repeated for other ray frustums to take into account of multi-path signals.

3. ACCELERATION TECHNIQUES

As shown in the previous section, the operations needed for ray frustums are mainly visibility tests. The acceleration schemes proposed in this paper are classified according to the stages in which they are applied. In the first stage, ray paths are found, and the frustums are generated recursively starting from the transmitter. The ray frustums accelerate this process in several aspects. During the generation of frustums, indices for triangles that belong to the frustum are stored for subsequent processes. The inclusion test for triangles can be efficiently carried out by a space partitioning method such as binary space partitioning, quad tree or octree. In order for each ray frustum to store indices for belonging triangles, it should be tested whether the triangles intersect with the ray frustum. With the triangles grouped by a space partitioning scheme such as quad tree or octree, the first stage of the inclusion tests determines whether a quad cell is included in the ray frustum. Then, it should be tested whether the triangles belonging to the quad cell are included in the frustum. The acceleration scheme reduces computational burden by a factor of 2^N, where N is the order of the quad tree. As in the previous section, the reduction by this partitioning has a limit since triangles tend to belong to several adjacent divisions for larger N. If a sphere that encircles a triangle is used for the inclusion test, the computational cost should be saved further.

Visible triangles are searched among the indexed triangles, which are seen from the apex of the ray frustum that represents a real or virtual source position. With the indices stored in the frustum data structure, the search process can be expedited since only those indexed triangles need to be tested instead of the whole triangles comprising environments.

If the indices are sorted by the distance from the apex of the frustum, as shown in Fig. 8, a computational burden can be reduced additionally by a factor of two. In determining whether a triangle is visible from the source, tests with triangles farther than the length of that line segment can be safely ignored with sorted triangles. While generating ray frustums, the distances of triangles from the apex can be calculated and stored in the computer memory.

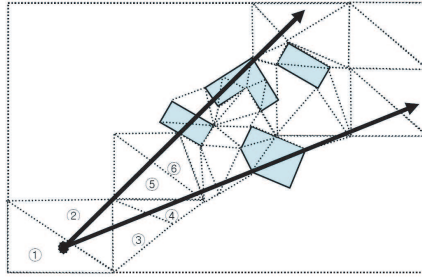After the whole ray frustums are generated, ray paths to

Figure 8. Indices for the triangles are sorted and numbered by the distance from the source point.

observation positions can be obtained. This process begins with the test of whether the position is included in a ray frustum. If a frustum includes an observation position, a backward ray tracing is necessary to determine an actual ray path from the transmitter to the observation point. This backward tracing can also be efficiently performed with ray frustums. Since each frustum holds indices for belonging triangles, intersection tests should be performed about those triangles only. Due to the narrow regions occupied by frustums, the number of indices is in general very small compared with the whole number of the triangles comprising the environment. With a large number of observation points and large computational burden, several additional acceleration schemes can be devised. The observation points can also be grouped by a space partition method, and it can collectively be tested whether they are contained in a certain ray frustum. At the same time, the numerous ray frustums can be indexed by a hashing function (Fig. 9). To obtain an electric field at an observation point, it should be tested whether the point is included in any of the whole ray frustums. To avoid unnecessary numerical calculations, the space that includes the whole environment is divided into lattice-like cells. Each cell is tested to determine whether it intersects any of the ray frustums. If so, the indices of those intersecting frustums are stored in the cell. With a hashing function that retrieves the belonging cell for an observation coordinate, tests for irrelevant frustums can be minimized.

4. CALCULATION OF RECEIVED POWER

The received power at an observation point is calculated with Friis transmission formula. For three dimensional modeling, three dimensional directivity data of transmitting and receiving antennas are required, which can be interpolated from measurement data along
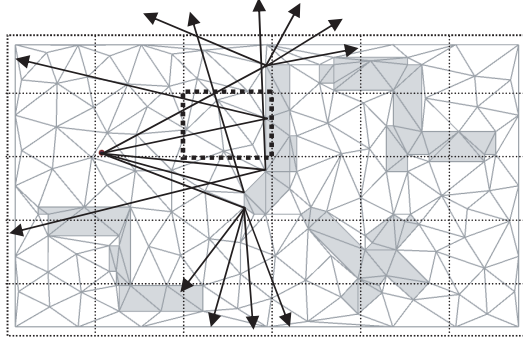
Figure 9. Observation points are grouped into lattices. The arrows represents bounding surface of ray frustums. The lattices contain indices for ray frustums that intersect them. If an observation point belongs to one lattice, the inclusion test needs to done for those indexed ray frustums only.

the E and H-planes [19].

If an observation point is included in a ray frustum, a ray path is formed, which traces back to the vertex of the frustum. If the ray hits the reflecting triangle or the diffracting edge that generates the frustum, the ray continues to trace back to the apex of the parent ray frustum. The process is recursively carried out until the ray hits the transmitting antenna. If the ray is intercepted by obstacles in the course of the ray tracing, the received power at the point is assumed to be zero. When the back-traced ray hits the source, the directivity of the transmitting antenna along the direction of the ray is utilized and the radiated electric field is obtained by Eq. (4).

$$\mathbf{E}_{\text{inc}} = \sqrt{\frac{\eta P_T}{4\pi} G_T\left(\theta_T, \phi_T\right)} \cdot \frac{\left(h_{T,v}\hat{\theta}_T + h_{T,h}\hat{\phi}_T\right)}{R} e^{-jkR} \qquad (4)$$

where P_T is the transmit power, and η is the wave impedance of the free space. The gain along the ray direction (θ_T, ϕ_T) is $G_T(\theta_T, \phi_T)$. Unit vectors $\hat{\theta}_T$ and $\hat{\phi}_T$ represent vectors along the elevation and azimuth directions, respectively. The values $h_{T,v}$ and $h_{T,h}$ represent the polarization components [20].

The incident electric field generated from the transmitting antenna undergoes reflection, transmission, and diffraction. Eq. (5) shows the received electric field of a ray that arrives at the receiving antenna after many combinations of reflections, diffractions and transmissions.

$$\mathbf{E}_{\text{received}} = \left[\prod A\left(s_{i-1}, s_i\right)\left(\bar{\mathbf{R}}_i \ \text{ or } \ \bar{\mathbf{T}}_i \ \text{ or } \ \bar{\mathbf{D}}_i\right) e^{-jks_i}\right] \bullet \mathbf{E}_{\text{inc}} \qquad (5)$$

where $A(s_{i-1}, s_i)$ is the divergence factor that accounts for the magnitude changes after i-th scattering. The dyadic quantities $\bar{\bar{\mathbf{R}}}_i$, $\bar{\bar{\mathbf{T}}}_i$, $\bar{\bar{\mathbf{D}}}_i$ are reflection, transmission, and diffraction.

The received voltage is the sum of multi-path signals that have propagated along actual ray paths. The voltage is obtained by Eq. (6).

$$V_R = \lambda \sqrt{\frac{Z_0}{4\pi}} \sum \sqrt{G_R(\theta_R, \phi_R)} \cdot \left[\left(h_{R,v} \hat{\theta}_R + h_{R,h} \hat{\phi}_R \right) \bullet \mathbf{E}_{\text{received}} \right] \quad (6)$$

where Z_0 is the characteristic impedance of a receiver, and $G_R(\theta_R, \phi_R)$ is the gain along the ray direction (θ_R, ϕ_R). Unit vectors $\hat{\theta}_R$ and $\hat{\phi}_R$ represent vectors along the elevation and azimuth directions seen from the receiving antenna coordinate, respectively. The values $h_{R,v}$ and $h_{R,h}$ represent the polarization components. The received power is obtained by Eq. (7).

$$P_R = |V_R|^2 / Z_0 \quad (7)$$

5. NUMERICAL RESULTS AND MEASUREMENTS

With the preceding acceleration algorithms, a computer code in C++ is developed to verify the efficiency. The code is implemented basically for three dimensional objects and the coordinate vectors have three components. To verify the ray frustum formulation, a comparison with the measurement is presented. The detail of the simulation process is as follows. First, with measured or simulated antenna radiation patterns, a three dimensional radiation pattern is interpolated and stored in the memory to save the calculation time. For convenience, bow-tie antennas of broad bandwidth at 2.6 GHz center frequency are used. The maximum gain of the antenna is 2.3 dBi. The material constants for the floor and the ceilings are $\varepsilon_r = 15$ and $\sigma = 0.1$ [S/m]. Those for the walls are $\varepsilon_r = 9$ and $\sigma = 0.02$ [S/m]. The test site is shown in Fig. 10. In the measurement, the transmitter emits 2.6 GHz continuous wave signal with strength -13.75 dBm. The combined gain of a receiver is 10 dB including cable losses. The same antennas are used for the transmitter and the receiver. The measurement is performed on reception points comprising two piece-wise linear paths with lengths of 48.6 m + 8.1 m. The height of the ceiling is 2.5 m. Received power levels are recorded on every 45 cm. The transmitter and receiver are at the height of 195 cm and 164 cm from the ground. The measurement was done at night with few people in the corridor. Fig. 11 compares the measured values with calculated results, showing good agreement and effectiveness of the formulations. The average of the differences between the measured data, and results of the simulation is -0.91 dB with the standard deviation 7.1 dB.
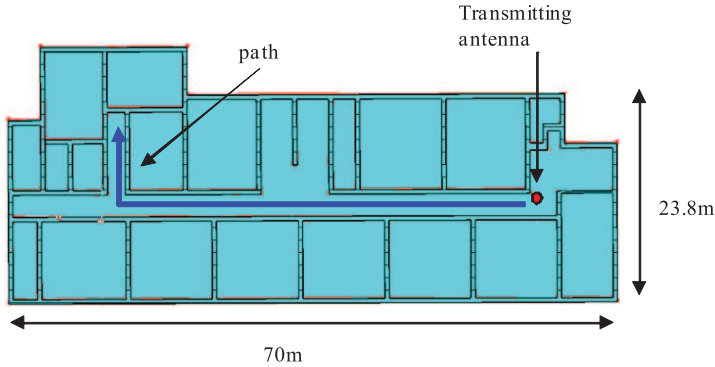
Figure 10. Layout of the test site used for verifying the effectiveness of a ray frustum model.
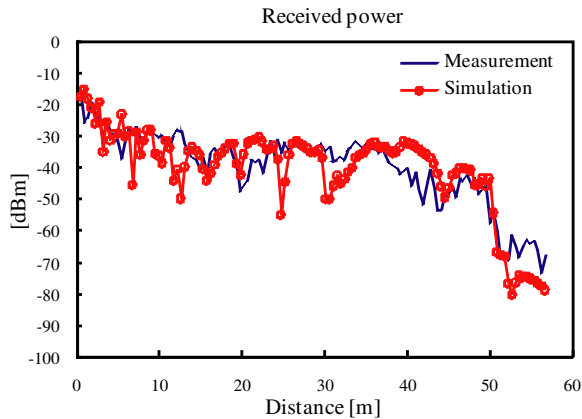

Figure 11. Received power data obtained by measurements along the path.

To examine the accelerating features of the ray frustum formulation, simulations are performed to obtain power levels at 40,000 receiver positions in an outdoor test site $(353\,\text{m} \times 293\,\text{m})$, as shown in Fig. 1. With generated ray frustum, each receiving position is tested to determine whether it is included in frustums. The receiving points are grouped by a quad tree with depth $0 \sim 7$. Fig. 12 shows computation times needed. Compared with no space partitioning, a reduction by an amount of 25% is achieved. Zero quad tree depth corresponds to no space partitioning. As the depths become larger than 4, the computation time due to partitioning increases. For the simulation,
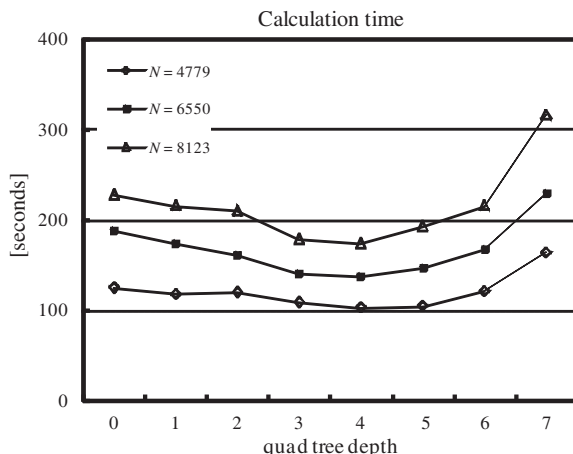
Figure 12. Effects of applying quad tree concept on the calculation times.
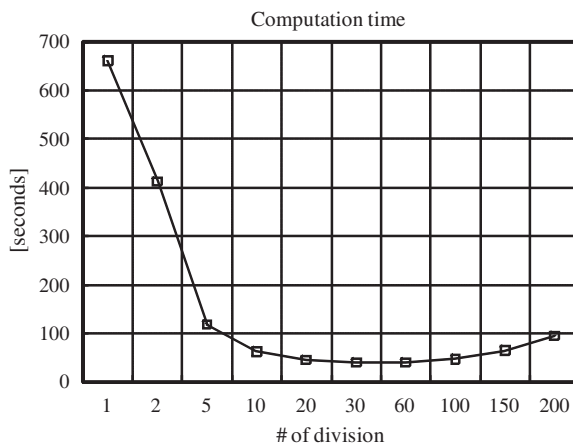

Figure 13. Effects of applying a hash function for the calculation of received power at 40,000 points. The environment is composed of 4779 triangular cells.

the outdoor test site is tessellated into $N = 4779$, 6550, 8123 triangles.

Figure 13 shows the effect of applying hash functions in indexing ray frustums. The environment is divided into regular grid structures. For each grid, indices for ray frustums intersecting the grid are recorded. To calculate a received power at an observation point, a hashing function is utilized to retrieve the grid that includes the reception point. Because the grid stores indices for intersecting
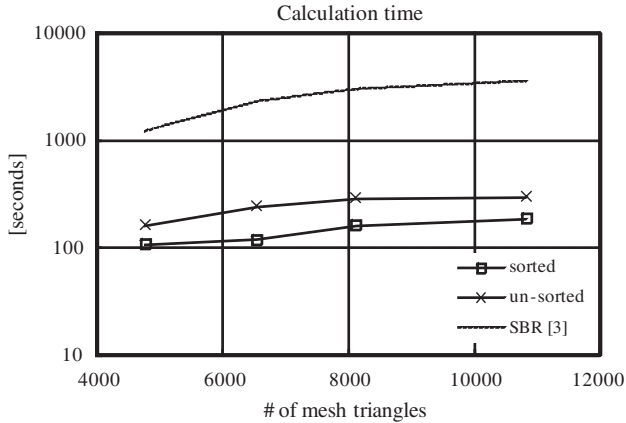
Figure 14. Elapsed computation time. A reduction by a factor of two is achieved by the triangle indices sorted by distances from the source positions of ray frustums.

frustums, inclusion tests should be performed only for those frustums, thus saving computation time. As in the quad tree partitioning, too dense grid increases computation time because nearby grid cells contain the same indices for frustums.

Figure 14 compares calculation times by ray frustums with sorted or unsorted indices for belonging triangles. For a reception position, visibility tests are done only for those triangles within the distance from the source to the receiving point, thus reducing computational cost by a factor of two.

6. CONCLUSION

In this paper, acceleration techniques combined with ray frustums are presented to reduce computation times for characterizing wireless channels. The visibility tests can be performed very efficiently with four kinds of ray frustums such as line of sight, reflection, transmission and diffraction frustums. A ray frustum collectively represents many possible ray paths, thus finding a ray path from a transmitter to a receiver quickly. The acceleration techniques such as quad tree, hashing function and sorting are combined with ray frustums. The presented techniques reduce the computation time by a factor of more than two, and the fast characterization of complex wireless communication environments is achieved.

REFERENCES

1. Gladstone, K. J. and J. P. McGeehan, "Computer simulation of multipath fading in the land mobile radio environment," *Proc. Inst. Elect. Eng.*, Pt. G, Vol. 27, No. 6, 323–330, 1980.

2. Lawton, M. C. and J. P. McGeehan, "The application of a deterministic ray launching algorithm for the prediction of radio channel characteristics in small-cell environments," *IEEE Trans. Veh. Tech.*, Vol. 43, No. 4, 955–969, 1994.

3. Chen, S.-H. and S.-K. Jeng, "An SBR/image approach for radio wave propagation in indoor environments with metallic furniture," *IEEE Trans. Antennas and Propag.*, Vol. 45, No. 1, 98–105, Jan. 1997.

4. Chen, C. H., C. L. Liu, C. C. Chiu, and T. M. Hu, "Ultra-wide band channel calculation by SBR/image techniques for indoor communication," *Journal of Electromagnetic Waves and Applications*, Vol. 20, No. 1, 41–51, 2006.

5. Wang, S., H. B. Lim, and E. P. Li, "An efficient ray-tracing method for analysis and design of electromagnetic shielded room systems," *Journal of Electromagnetic Waves and Applications*, Vol. 19, No. 15, 2059–2071, 2005.

6. Catedra, M. F., J. Perez, F. S. Adana, and O. Gutierrez, "Efficient ray-tracing techniques for three dimensional analyses of propagation in mobile communications: Application to picocell and microcell scenarios," *IEEE Antennas and Propag. Magazine*, Vol. 40, No. 2, 15–28, 1998.

7. Son, H.-W. and N.-H. Myung, "A deterministic ray tube method for microcellular wave propagation prediction model," *IEEE Trans. Antennas and Propag.*, Vol. 47, No. 8, 1344–1350, 1999.

8. Yang, C.-F. and B.-C. Wu, "A ray-tracing/PMM hybrid approach for determining wave propagation through periodic structures," *IEEE Trans. Veh. Tech.*, Vol. 50, No. 3, 791–795, 2001.

9. Schuster, J. W. and R. J. Luebbers, "Comparison of GTD and FDTD predictions for UHF radio wave propagation in a simple outdoor urban environment," *IEEE Antennas and Propag. Society International Symposium*, Vol. 3, 2022–2025, 1997.

10. Yun, Z., Z. Zhang, and M. F. Iskander, "A ray-tracing method based on the triangular grid approach and application to propagation prediction in urban environments," *IEEE Trans. Antennas and Propag.*, Vol. 50, No. 5, 750–758, 2002.

11. Bang, J. K., B. C. Kim, S. H. Suk, K. S. Jin, and H. T. Kim, "Time consumption reduction of ray tracing for RCS prediction using

efficient grid division and space division algorithms," *Journal of Electromagnetic Waves and Applications*, Vol. 21, No. 6, 829–840, 2007.

12. Jin, K. S., T. I. Suh, S. H. Suk, B. C. Kim, and H. T. Kim, "Fast ray tracing using a space-division algorithm for RCS prediction," *Journal of Electromagnetic Waves and Applications*, Vol. 20, No. 1, 119–126, 2006.

13. Tao, Y. B., H. Lin, and H. J. Bao, "KD-tree based fast ray tracing for RCS prediction," *Progress In Electromagnetics Research*, PIER 81, 329–341, 2008.

14. Alvar, N. S., A. Ghorbani, and H. Amindavar, "A novel hybrid approach to ray-tracing acceleration based on pre-processing and bounding volumes," *Progress In Electromagnetics Research*, PIER 82, 19–32, 2008.

15. Speer, L. R., T. D. DeRose, and B. A. Barsky, "A theoretical and empirical analysis of coherent ray tracing," *Proceedings Graphics Interface*, 11–25, 1985.

16. Suzuki, H. and A. S. Mohan, "Frustum ray tracing technique for high spatial resolution channel characteristic map," *IEEE Radio and Wireless Conference*, 253–256, 1998.

17. Lauterbach, C., A. Chandak, and D. Manocha, "Interactive sound rendering in complex and dynamic scenes using frustum tracing," *IEEE Trans. Visualization and Computer Graphics*, Vol. 13, No. 6, 1672–1679, 2007.

18. Burnside, W. D. and K. W. Burgener, "High frequency scattering by a thin lossless dielectric slab," *IEEE Trans. Antennas and Propag.*, Vol. 31, No. 1, 104–110, Jan. 1983.

19. Gil, F., A. R. Claro, J. M. Ferreira, C. Pardelinha, and L. M. Correia, "A 3D interpolation method for base-station-antenna radiation patterns," *IEEE Antennas and Propag. Magazine*, Vol. 43, No. 2, 132–137, 2001.

20. Adana, F. S., O. G. Blanco, I. G. Diego, J. P. Arriaga, and M. F. Catedra, "Propagation model based on ray tracing for the design of personal communication systems in indoor environments," *IEEE Trans. Vehicular Tech.*, Vol. 49, No. 6, 2105–2112, Nov. 2000.